Associated production of a graviton with an e^+e^- pair via photon-photon collisions at a linear collider

Zhou Ya-Jin, Ma Wen-Gan, Han Liang, and Zhang Ren-You

Department of Modern Physics, University of Science and Technology of China (USTC), Hefei, Anhui 230026, People's Republic of China

(Received 29 April 2007; published 24 September 2007)

We investigate the process $\gamma\gamma \to e^+e^-G_n$ at the future International Linear Collider (ILC), where G_n is the Kaluza-Klein graviton in the large extra dimension model. When the fundamental energy scale is of a few TeV, the cross section of this process can reach several hundred fb at a photon-photon collider with $\sqrt{s} = 500$–1000 GeV, and the cross section in the $J = 2$ polarized photon collision mode is much larger than that in the $J = 0$ polarized photon collision mode. We present strategies to distinguish the graviton signal from numerous SM backgrounds, and find that the graviton signal with extra dimensions $\delta = 3$ can be detected when $M_S \leq 2.67(1.40)$ TeV and $\gamma\gamma$ center of mass system energy $\sqrt{s} = 1000(500)$ GeV in unpolarized photon collision mode, while the detecting upper limit can be increased to 2.79(1.44) TeV in $+-$ ($\lambda_1 = 1$, $\lambda_2 = -1$) polarized photon collision mode (with photon polarization efficiency $P_\gamma = 0.9$).

DOI: 10.1103/PhysRevD.76.054003 PACS numbers: 04.50.+h, 13.85.Qk, 13.88.+e

I. INTRODUCTION

The hierarchy problem of the standard model (SM) strongly suggests new physics at TeV scale, and the idea of extra dimensions (ED) [1–6] might provide a solution to this problem. The large extra dimension model (LED, also called ADD model) [1] is the most promising one among the various extra dimension models. It introduces a fundamental scale M_S in D ($D = 4 + \delta$) dimension, which is at the TeV scale, to unify the gravitational and gauge interactions. The usual Plank scale $M_P = 1/\sqrt{G_N} \sim 1.22 \times 10^{19}$ GeV (where G_N is Newton's constant) is related to M_S through

$$M_P^2 \sim M_S^{2+\delta} R^\delta, \tag{1.1}$$

where δ is the number of extra dimensions, and $R/2\pi$ is the radius of the compactified space. The fundamental scale M_S can be at TeV scale if R is large enough, which is at the same order with electroweak scale, thus the hierarchy problem is settled naturally.

From Eq. (1.1) we can estimate the value of R. If we set $M_S = 1$ TeV and $\delta = 1$, we have $R \sim 10^{13}$ cm, which is obviously ruled out since it would modify Newton's law of gravity at solar-system distances. For $\delta = 2$, there exists $R \sim 1$ mm. The latest torsion-balance experiments predict that an extra dimension must have a size $R \leq 44$ μm [7], so $\delta = 2$ must be ruled out too. When $\delta \geq 3$, where $R \sim 1$ nm, it is possible to detect the graviton signal at high energy colliders.

The large extra dimension model becomes an attractive extension of the SM because of its possible testable consequences. As Arkani-Hamed, Dimopoulos, and Dvali [1] proposed, the SM particles exist in the usual $(3 + 1)$-dimensional space, while gravitons can propagate in a higher-dimensional space. The picture of a massless graviton propagating in D-dimensions is equal to the picture that numerous massive Kaluza-Klein gravitons propagate in 4 dimensions. So we can expect that even though the gravitational interactions in the 4 space-time dimensions are suppressed by a factor of $1/M_P$, it can be compensated by these numerous KK states. So in either the case of real graviton emission or the case of virtual graviton exchange, it is shown [8,9] that, after summing over the KK states, the Plank mass M_P cancels out of the cross section, and we can obtain an interaction strength comparable to the electroweak strength.

The CERN Large Hadron Collider (LHC) and the planned International Linear Collider (ILC) both provide ideal grounds for testing SM and probing possible physics beyond SM. However, the ILC has more advantage in testing extra dimensions. Even though the LHC and ILC have comparable search reaches for the direct KK graviton production, the LHC is hampered by theoretical ambiguities due to a breakdown of the effective theory when the parton-level center-of-mass energy exceeds M_S [10]. Furthermore, the ILC has a cleaner environment than LHC, so it is much easier to separate the ED signals. In the first stage of the ILC, the center-of-mass energy will reach 500 GeV and the luminosity, $\mathcal{L}$ will be 500 fb^{-1} for the first four years running. The second phase foresees an energy upgrade to about 1 TeV and a luminosity to one ab^{-1} in 3–4 years running. ILC can also be operated in $\gamma\gamma$ and $e\gamma$ modes, where high energy photon beams can be obtained and easily polarized via laser backscattering of the e^+e^- beams.

Since gravitons interact with detectors weakly, they are not detectable and will give rise to missing energy, so the suggested graviton signal at LC would be associated production of graviton with SM particles. The most frequently discussed processes at LC are associated production of graviton with a photon ($e^+e^- \to \gamma G_n$) [8,9,11,12], a fermion pair ($e^+e^- \to e^+e^-G_n$) [13,14], a Z boson ($e^+e^- \to ZG_n$) [15], or a fermion at $e\gamma$ mode ($e\gamma \to fG_n$) [14].

Generally, the e^+e^- collider has the advantage that the luminosity is higher than the $\gamma\gamma$ collider, for example, $\mathcal{L}_{\gamma\gamma} \sim 0.15 - 0.2\mathcal{L}_{e^+e^-}$ or even $0.3 - 0.5\mathcal{L}_{e^+e^-}$ (through reducing emittance in the damping rings) [16], but the polarization technique for the photon is much simpler than the electron. Through calculation, we find that the W-induced SM background can be reduced after polarization. Furthermore, $\gamma\gamma \to l^+l^-$ $(l = e, \mu)$ is the best process for the measurement of the $\gamma\gamma$ luminosity [17], so it is convenient to select events with missing energy from these beam calibration processes. For these reasons, we studied the associated production of graviton with an e^+e^- pair at a LC in $\gamma\gamma$ collision mode, i.e., the process $\gamma\gamma \to e^+e^-G_n$. The paper is arranged as follows: in Sec. II, we present the analytical and numerical calculation of the cross section. The signal analysis and background elimination strategies are given in Sec. III. Finally, a short summary is given.

II. CROSS SECTION CALCULATIONS

A. Analytical calculations

We denote the process of a graviton production associated with the e^+e^- pair as

$$\gamma(p_1, \lambda_1, \nu_1)\gamma(p_2, \lambda_2, \nu_2) \to G_n(k_3, \lambda_s, \mu_1, \mu_2)e^-(k_4)e^+(k_5), \quad (2.1)$$

where p_i and k_i are the momenta of the incoming photons and outgoing particles, respectively, $\lambda_{1,2}$, λ_s are the polarizations of incoming photons and final graviton, and ν_i, μ_i are the Lorentz indices of the photons and graviton, respectively. There are 14 Feynman diagrams contributing to this process at the tree level, which are representatively shown in Fig. 1. The possible corresponding Feynman diagrams created by exchanging the initial photons and the graviton radiated from the final positron also involved in our calculation. Figure 1(a) gives the Feynman diagram where a graviton emitted from a vertex, and there are four such kinds of diagrams involved. Figure 1(b) represents a graviton emitted from one of the initial photons via triple vertex, and there are 4 such kinds of diagrams. Figure 1(c) represents a graviton emission from the final electrons/positron, and there are also 4 diagrams included. Figure 1(d) shows the diagram of a graviton emission from the electron propagator, and there are two such diagrams. The Feynman diagrams mediated by a graviton are not figured in Fig. 1 and also not included in our calculation because of their negligible contributions within the energy regions considered in this paper.

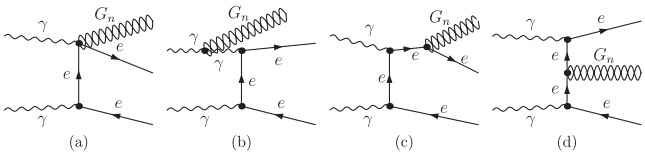

FIG. 1. Representative diagrams for the process $\gamma\gamma \to e^+e^-G_n$.

In our calculation we consider both the spin-0 and spin-2 graviton emission processes, and find that, in the case of scalar graviton emission, only the electron-mass dependent terms give contributions to the amplitude, just like in the case $f\bar{f} \to V + G_n$, which was mentioned in Ref. [9]. So we are only interested in the spin-2 component of the Kaluza-Klein (KK) states. We use the Feynman rules presented in Refs. [8,9] to calculate the amplitude of process $\gamma\gamma \to e^+e^-G_n$.

The gravitational coupling $\kappa \equiv \sqrt{16\pi G_N}$ can be expressed in terms of the fundamental scale M_S and the size of the compactified space R by

$$\kappa^2 R^\delta = 16\pi(4\pi)^{\delta/2}\Gamma(\delta/2)M_S^{-(\delta+2)}. \quad (2.2)$$

Here we give the amplitudes for the representative diagrams shown in Fig. 1(a)–1(d), separately:

$$\mathcal{M}_a = \frac{ie^2\kappa}{4}\frac{1}{(k_5 - p_2)^2}\epsilon_{\nu_1}(p_1)\epsilon_{\nu_2}(p_2)\epsilon_{\mu_1\mu_2}(k_3)\bar{u}(k_4) \times (\gamma_{\mu_2}\eta_{\mu_1\nu_1} + \gamma_{\mu_1}\eta_{\mu_2\nu_1} - 2\gamma_{\nu_1}\eta_{\mu_1\mu_2}) \times (\not{p}_2 - \not{k}_5)\gamma_{\nu_2}v(k_5), \quad (2.3)$$

$$\mathcal{M}_b = \frac{ie^2\kappa}{2}\frac{1}{(p_1 - k_3)^2}\frac{1}{(k_5 - p_2)^2}\epsilon_{\nu_1}(p_1)\epsilon_{\nu_2}(p_2)\epsilon_{\mu_1\mu_2}(k_3)\bar{u}(k_4)\gamma_\alpha(\not{p}_2 - \not{k}_5)\gamma_{\nu_2}v(k_5)\Big\{\frac{1}{2}\eta_{\mu_1\mu_2}[-p_{1\alpha}(p_1 - k_3)_{\nu_1} + p_1\cdot(p_1 - k_3)\eta_{\nu_1\alpha}] - \eta_{\nu_1\alpha}p_{1\mu_1}(p_1 - k_3)_{\mu_2} + \eta_{\mu_1\nu_1}[-p_1\cdot(p_1 - k_3)\eta_{\mu_2\alpha} + p_{1\alpha}(p_1 - k_3)_{\mu_2}] - \eta_{\mu_1\alpha}p_{1\mu_2}(p_1 - k_3)_{\nu_1} + \frac{1}{2}\eta_{\mu_2\mu_1}[-p_{1\alpha}(p_1 - k_3)_{\nu_1} + p_1\cdot(p_1 - k_3)\eta_{\nu_1\alpha}] - \eta_{\nu_1\alpha}p_{1\mu_2}(p_1 - k_3)_{\mu_1} + \eta_{\mu_2\nu_1}[-p_1\cdot(p_1 - k_3)\eta_{\mu_1\alpha} + p_{1\alpha}(p_1 - k_3)_{\mu_1}] + \eta_{\mu_2\alpha}p_{1\mu_1}(p_1 - k_3)_{\nu_1}\Big\}, \quad (2.4)$$

$$\mathcal{M}_c = -\frac{ie^2\kappa}{8}\frac{1}{(k_3 + k_4)^2}\frac{1}{(p_2 - k_5)^2}\epsilon_{\nu_1}(p_1)\epsilon_{\nu_2}(p_2)\epsilon_{\mu_1\mu_2}(k_3)\bar{u}(k_4)[\gamma_{\mu_2}(k_3 + 2k_4)_{\mu_1} + \gamma_{\mu_1}(k_3 + 2k_4)_{\mu_2} - 2\eta_{\mu_1\mu_2}(\not{k}_3 + 2\not{k}_4)](\not{k}_3 + \not{k}_4)\gamma_{\nu_1}(\not{p}_2 - \not{k}_5)\gamma_{\nu_2}v(k_5), \quad (2.5)$$

$$\mathcal{M}_d = -\frac{ie^2\kappa}{8}\frac{1}{(p_1-k_4)^2}\frac{1}{(p_2-k_5)^2}\epsilon_{\nu_1}(p_1)\epsilon_{\nu_2}(p_2) \times \epsilon_{\mu_1\mu_2}(k_3)\bar{u}(k_4)\gamma_{\nu_1}(\not{k}_4-\not{p}_1)[\gamma_{\mu_2}(k_3+2k_4-2p_1)_{\mu_1} + \gamma_{\mu_1}(k_3+2k_4-2p_1)_{\mu_2} - 2\eta_{\mu_1\mu_2}(\not{k}_3+2\not{k}_4-2\not{p}_1)] \times(\not{p}_2-\not{k}_5)\gamma_{\nu_2}v(k_5). \quad (2.6)$$

The amplitudes for other diagrams can be easily obtained by changing the corresponding momenta in these expressions.

The spin-averaged amplitude squared for the process is expressed as follows:

$$\overline{\sum_{\text{spins}}}|\mathcal{M}|^2 = \frac{1}{4}\sum_{\text{spins}}\left(\sum_{i=1}^{14}\mathcal{M}_i\right)^{\dagger}\left(\sum_{i=1}^{14}\mathcal{M}_i\right), \quad (2.7)$$

where $\mathcal{M}_i$ represents the amplitude for the ith Feynman diagram. The bar over summation means taking the average over initial photon spin states. By taking the summation over the polarizations of the spin-2 graviton tensor wave functions, we have [8,9]

$$\sum_{\lambda_s=1}^{5}\epsilon_{\mu\nu}(k,\lambda_s)\epsilon^*_{\alpha\beta}(k,\lambda_s) = P_{\mu\nu\alpha\beta}(k), \quad (2.8)$$

where $P_{\mu\nu\alpha\beta}$ is

$$P_{\mu\nu\alpha\beta} = \frac{1}{2}(\eta_{\mu\alpha}\eta_{\nu\beta}+\eta_{\mu\beta}\eta_{\nu\alpha}-\eta_{\mu\nu}\eta_{\alpha\beta}) - \frac{1}{2m^2}(\eta_{\mu\alpha}k_\nu k_\beta+\eta_{\nu\beta}k_\mu k_\alpha+\eta_{\mu\beta}k_\nu k_\alpha + \eta_{\nu\alpha}k_\mu k_\beta)+\frac{1}{6}\left(\eta_{\mu\nu}+\frac{2}{m^2}k_\mu k_\nu\right) \times\left(\eta_{\alpha\beta}+\frac{2}{m^2}k_\alpha k_\beta\right). \quad (2.9)$$

In practical experiments, the contributions of the different Kaluza-Klein modes have to be summed up. For not too large extra dimensions δ, the mass spacing of these KK states is much smaller than the physical scale, so it is convenient to replace the summation over the KK states by a continuous integration:

$$\sigma = \sum_n \sigma_m \rightarrow \int_0^{\sqrt{s}}\rho(m)\sigma_m dm, \quad (2.10)$$

where $\rho(m)$ is the density of states, which is

$$\rho(m) = \frac{2R^\delta m^{\delta-1}}{(4\pi)^{\delta/2}\Gamma(\delta/2)} = \frac{32\pi m^{\delta-1}}{\kappa^2 M_S^{\delta+2}}. \quad (2.11)$$

σ_m in Eq. (2.10) is the cross section for a definite KK state, and it can be expressed as the integration over the phase space of three-body final states:

$$\sigma_m = \frac{(2\pi)^4}{4|\vec{p}_1|\sqrt{s}}\int d\Gamma_3\overline{\sum_{\text{spins}}}|\mathcal{M}|^2. \quad (2.12)$$

The integration is performed over the three-body phase space of final particles $e^+e^-G_n$. The phase-space element $d\Gamma_3$ is defined by

$$d\Gamma_3 = \delta^{(4)}\left(p_1+p_2-\sum_{i=3}^{5}k_i\right)\prod_{j=3}^{5}\frac{d^3\boldsymbol{k}_j}{(2\pi)^3 2E_j}. \quad (2.13)$$

In the process of numerical calculation, the integration over the mass of the KK states and over the phase space can be done at the same time.

B. Numerical results

In this subsection we present the numerical results of the total cross section for the process $\gamma\gamma \rightarrow e^+e^-G_n$. The value of the fine structure constant α is taken as $1/128$ [18]. In the calculations for this process with TeV scale colliding energy, we ignore the masses of electron and positron. To remove the singularities which arise when the final massless electron/positron is collinear with the photon beam, we set a small cut on the angle between electron/positron and one of the incoming photons, which is $2^\circ < \theta_{e\gamma} < 178^\circ$.

The incoming γ beams have five polarization modes: $++$, $+-$, $-+$, $--$, and unpolarized collision modes, for example, the notation of $+-$ represents helicities of the two initial photons being $\lambda_1 = 1$ and $\lambda_2 = -1$. In Table I we give the total cross sections of the graviton emitting process accompanied with an e^+e^- pair considered in this paper, with different numbers of extra dimensions, $\gamma-\gamma$ center of mass system (c.m.s.) energy, and photon polarization modes. The polarization efficiency of photon $P_\gamma(P_\gamma \equiv \frac{N_+-N_-}{N_++N_-})$ is assumed to be 0.9. Since the cross sections of the $+-$ and $-+$ photon polarizations (i.e., $J=2$) are equal, and also the cross sections of the $++$ and $--$ photon polarizations (i.e., $J=0$) are the same, we only give the total cross sections in three cases: $+-$, $++$, and unpolarized photons.

From Table I we can see that the cross section can reach several hundred fb when the $\gamma-\gamma$ c.m.s. energy is 1 TeV. The larger the number of extra dimensions is, the smaller the cross section becomes. It is obvious that the cross sections in the case with $+-$ polarized incoming photons

TABLE I. Total cross sections for the process $\gamma\gamma \rightarrow e^+e^-G_n$, with and without photon polarization. M_S is set to be 1 TeV, the polarization efficiency $P_\gamma = 0.9$, and the cross sections are in fb.

$\sqrt{s}$ [GeV]		$\delta=3$	$\delta=4$	$\delta=5$	$\delta=6$
500	unpolarized	46.46	13.92	4.692	1.700
	$+-$	60.01	19.35	6.853	2.576
	$++$	32.91	8.493	2.532	0.821
1000	unpolarized	371.7	222.7	150.1	108.8
	$+-$	480.8	309.6	219.3	164.9
	$++$	262.6	135.8	80.93	52.75

are much larger than those in the case in $++$ polarized photon-photon collision. This is because the spin of the emitted graviton is 2, so it is much easier for $J = 2$ initial states to generate a spin-2 graviton. This feature becomes more evident when the number of extra dimensions becomes larger. When $\delta = 6$, the cross section with the $+-$ polarized photons can reach 3 times that with the $++$ polarized photons. We also find that the cross sections at $\sqrt{s} = 1$ TeV are much larger than those at $\sqrt{s} = 500$ GeV. To show the relationship between the cross section and the $\gamma - \gamma$ c.m.s energy more clearly, we depict two curves for the production rate of the process $\gamma\gamma \to e^+e^-G_n$ as the function of $\sqrt{s}$ in Fig. 2, with $M_S = 1.5$ TeV and the incoming photons being unpolarized and $+-$ polarized ($P_\gamma = 0.9$), respectively. Since the perturbative theory is only applicable when $\sqrt{s} \leq M_S$, we take the $\sqrt{s} < 1.5$ TeV in Fig. 2. The figure shows that the cross sections go up quickly with the increment of $\sqrt{s}$, because there are more KK states contributing to the cross section. The cross section is rather small at low $\sqrt{s}$ because of phase-space suppression. At the same time, we can see that the $+-$ polarization photon beams can strongly enhance the cross section.

III. SIGNAL ANALYSIS

Since the graviton interacts with materials weakly, an emitted graviton cannot be detected in the experiment. Therefore, in the measurement of the process $\gamma\gamma \to e^+e^-G_n$, the existence of a graviton manifests as the phenomenon of missing energy. The signature for this process is

$$\gamma\gamma \to e^+e^- + \text{missing energy}. \tag{3.1}$$

So the processes of the form $\gamma\gamma \to e^+e^-$(neutrinos), where the neutrinos can be of any generation, are SM background which can effect the discrimination of the graviton. The main SM background processes at the lowest order for the signal of $\gamma\gamma \to e^+e^-G_n$ are

$$\gamma\gamma \to e^+e^- \tag{3.2}$$

$$\gamma\gamma \to e^+e^-Z \to e^+e^-(\nu\bar{\nu}) \tag{3.3}$$

$$\gamma\gamma \to W^+W^- \to (e^+\nu_e)(e^-\bar{\nu}_e) \tag{3.4}$$

$$\gamma\gamma \to \tau^+\tau^- \to (e^+\nu_e\bar{\nu}_\tau)(e^-\bar{\nu}_e\nu_\tau). \tag{3.5}$$

All these processes contribute a formidable background to the graviton signal of $\gamma\gamma \to e^+e^-G_n$. However, a reasonable set of kinematic cuts enables us to distinguish the suggested signal from the backgrounds. First, the electron-positron pair in the process (3.2) is collinear, so we can remove the $\gamma\gamma \to e^-e^+$ background totally by putting a cut on the angle between the final electron and positron. The contributions from $\gamma\gamma \to e^+e^-Z$ can be expressed as

$$\begin{aligned}\sigma_{e^+e^-Z} &= \sigma(\gamma\gamma \to e^+e^-Z) \times Br(Z \to \nu\bar{\nu}) \\ &= \sigma(\gamma\gamma \to e^+e^-Z) \times 20.0\%\end{aligned} \tag{3.6}$$

$$= \begin{cases} 10.65 \text{ fb} & (\text{for } \sqrt{s} = 500 \text{ GeV}); \\ 4.17 \text{ fb} & (\text{for } \sqrt{s} = 1000 \text{ GeV}). \end{cases} \tag{3.7}$$

The primary dominant backgrounds should be the $\gamma\gamma \to W^+W^-$ and $\gamma\gamma \to \tau^+\tau^-$ processes, which are called as WW- and $\tau\tau$-background, respectively, in the following discussion. Their contributions are given by

$$\begin{aligned}\sigma_{WW} &= \sigma(\gamma\gamma \to W^+W^-) \times (Br(W \to e\nu_e))^2 \\ &= \sigma(\gamma\gamma \to W^+W^-) \times (10.75\%)^2\end{aligned} \tag{3.8}$$

$$= \begin{cases} 1011 \text{ fb} & (\text{for } \sqrt{s} = 500 \text{ GeV}) \\ 1019 \text{ fb} & (\text{for } \sqrt{s} = 1000 \text{ GeV}). \end{cases} \tag{3.9}$$

$$\begin{aligned}\sigma_{\tau\tau} &= \sigma(\gamma\gamma \to \tau^+\tau^-) \times (Br(\tau \to e\nu_e\nu_\tau))^2 \\ &= \sigma(\gamma\gamma \to \tau^+\tau^-) \times (17.84\%)^2\end{aligned} \tag{3.10}$$

$$= \begin{cases} 243.1 \text{ fb} & (\text{for } \sqrt{s} = 500 \text{ GeV}) \\ 62.36 \text{ fb} & (\text{for } \sqrt{s} = 1000 \text{ GeV}). \end{cases} \tag{3.11}$$

We developed an event generator program for the process $\gamma\gamma \to e^+e^-G_n$ and $\gamma\gamma \to e^+e^-Z$, and the WW- and

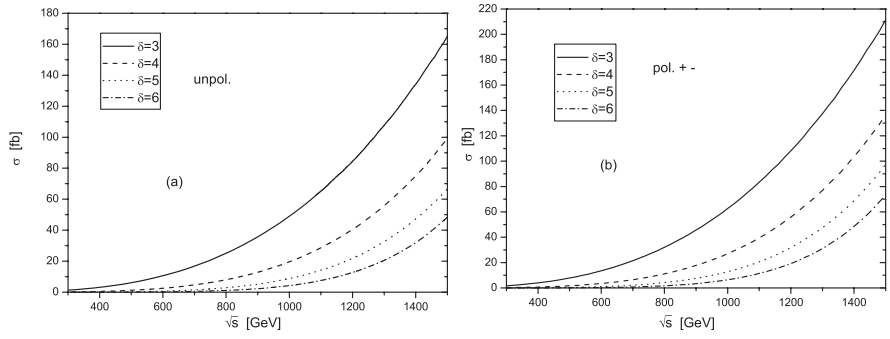

FIG. 2. The cross section for process $\gamma\gamma \to e^+e^-G_n$ as the functions of $\gamma\gamma$ colliding energy $\sqrt{s}$, with $M_S = 1.5$ TeV: (a) for the unpolarized photon-photon collision, (b) for $+-$ polarized photon-photon collision with $P_\gamma = 0.9$.

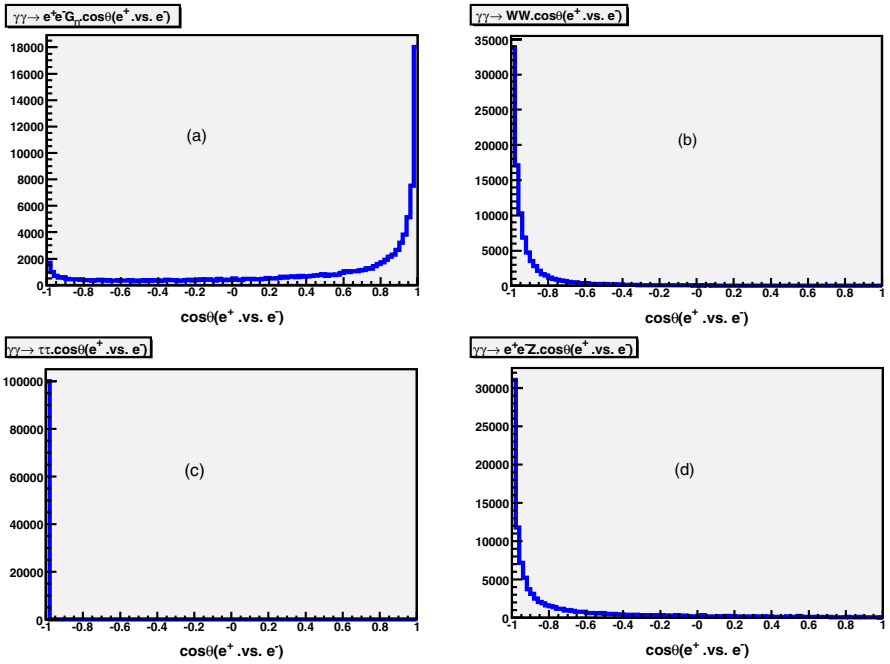

FIG. 3 (color online). Distributions of the open angle between the electron and positron for the signal process when extra dimensions $\delta = 3$ and the background processes. The $\gamma\gamma$ c.m.s. energy is 1 TeV and M_S is set to be 1 TeV.

$\tau\tau$-background events are generated by adopting the PYTHIA package [19]. In Fig. 3 we depict the Monte Carlo distributions of the open angle between electron and positron θ_{ee} for the signal process $\gamma\gamma \to e^+e^-G_n$ and background processes ($\gamma\gamma \to e^+e^-Z$, $\gamma\gamma \to W^+W^-$, and $\gamma\gamma \to \tau\tau$) separately, with the $\gamma\gamma$ colliding energy $\sqrt{s} = 1$ TeV. The θ_{ee} distributions for the signal process $\gamma\gamma \to e^+e^-G_n$, $\gamma\gamma \to e^+e^-Z$, WW- and $\tau\tau$-background processes at $\sqrt{s} = 500$ GeV have the similar line shapes with the corresponding ones at $\sqrt{s} = 1000$ GeV as shown in Fig. 3. The back-to-back feature of the final e^+e^- pair for the main background processes is shown evidently in Fig. 3, especially for the process $\gamma\gamma \to \tau\tau$. If we put a suitable cut on the open angle between the electron and positron $\theta_{ee}^{\rm cut}$, it is possible to remove the background events including also the $\gamma\gamma \to e^+e^-$ process from the signals of $\gamma\gamma \to e^+e^-G_n$ at $\sqrt{s} = 1000$ GeV. But in the case of $\sqrt{s} = 500$ GeV, the $\theta_{ee}^{\rm cut}$ is not enough to eliminate the WW-background process. In Fig. 4 we show the simulating distributions of the missing invariant mass of the signal process $\gamma\gamma \to e^+e^-G_n$ and the WW-background process with extra dimensions $\delta = 3$, $\sqrt{s} = 500$ GeV, and $M_S = 1$ TeV after applying $CUT1$ which is introduced below, and find that an extra missing invariant mass cut can reduce more WW-background events.

From the above discussion, we choose the off-line event selection criteria as follows:

(1) To take into account the detector acceptance, first, we demand that the angle between electron (positron) and the photon beam should be in the range $5° < \theta_{e\gamma} < 175°$. Second, the transverse momentum of the electron (positron) should satisfy $p_T^e > 5$ GeV. We also demand that the electron (positron) energy $E_e > 1$ GeV. To separate the electron and

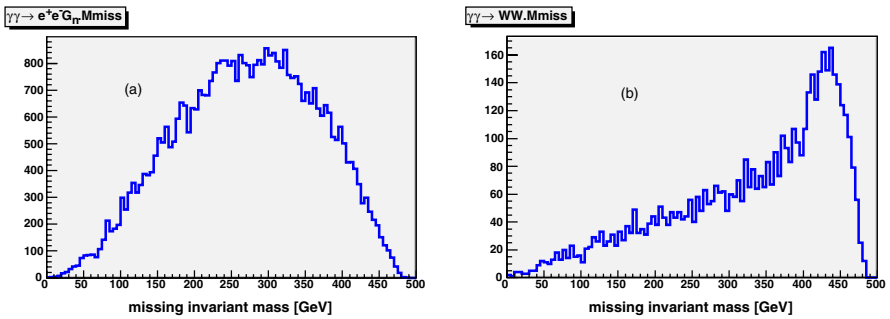

FIG. 4 (color online). Distributions of the missing invariant mass of the signal process and the WW-background process after applying $CUT1$ when extra dimensions $\delta = 3$. The $\gamma\gamma$ c.m.s. energy is 500 GeV and M_S is set to be 1 TeV.

TABLE II. Event selection on background and signal ($\delta = 3$) with the unpolarization case.

	$\sqrt{s} = 500$ GeV				$\sqrt{s} = 1000$ GeV			
	$e^+e^-G_n$	WW	$\tau\tau$	e^+e^-Z	$e^+e^-G_n$	WW	$\tau\tau$	e^+e^-Z
N before cut	4646	101 100	24 310	1065	37 170	101 900	6236	417
N after $CUT1$	1805	5402	0	86	17 790	649	0	31
N after $CUT2$	1616	3427	0	86	...	...	...	...
Efficiency ϵ	34.8%	3.39%	0%	8.08%	47.9%	0.64%	0%	7.43%
SB		27.26				682.2		

positron tracks, we demand that the open angle between electron and positron θ_{ee} should be larger than 5°. On the other hand, to eliminate the WW, $\tau\tau$, $\gamma\gamma \to e^+e^-$, and e^+e^-Z background, we set a more strict cut on θ_{ee}, i.e., $5° < \theta_{ee} < \theta_{ee}^{\rm cut} = 90°$. We denote these cuts as $CUT1$ set, which are expressed as

$$5° < \theta_{e\gamma} < 175°, \qquad p_T^e > 5 \text{ GeV},$$
$$E_e > 1 \text{ GeV}, \quad \text{and} \quad 5° < \theta_{ee} < \theta_{ee}^{\rm cut} = 90°.$$

(2) For $\sqrt{s} = 500$ GeV, a cut on the missing invariant mass is needed, which is denoted as $CUT2$:

$$M_{\rm miss} < 400 \text{ GeV}.$$

Taking the photon integrated luminosity to be $\mathcal{L} = 100^{-1}$ fb, we present in Table II the event numbers of the signal process with $\delta = 3$ and $M_S = 1$ TeV and the background processes after each step of cut, the event selection efficiency after cuts, and the significance of signal over background. Here the event selection efficiency is defined as the event numbers after cuts divided by the event numbers before any cut. The significance of signal over background (SB) is defined as

$$\text{SB} = \frac{N_{\rm signal}}{\sqrt{N_{\rm background}}} = \frac{\sigma_S^{CUT} \cdot \mathcal{L}_{\gamma\gamma}}{\sqrt{\sigma_B^{CUT} \cdot \mathcal{L}_{\gamma\gamma}}} = \frac{\sigma_S^{CUT}}{\sqrt{\sigma_B^{CUT}}} \cdot \sqrt{\mathcal{L}_{\gamma\gamma}}. \tag{3.12}$$

Here we have discussed the case of unpolarized photons. In Sec. II we show that the cross section for the signal process with $J = 2$ polarized photons is much larger than that with $J = 0$ photons. On the contrary, we find that, with the incoming photon polarizations, the cross section for the primary SM background process $\gamma\gamma \to W^+W^-$ is suppressed in the colliding case with $J = 2$. So it will be much easier to eliminate SM backgrounds in case of $J = 2$ collision mode. Using the similar signal analysis procedure with above, we obtain the data with the $+-$ polarized case (with $P_\gamma = 0.9$), and list them in Table III.

Notice that the data in Tables II and III are obtained by taking $M_S = 1$ TeV. The cross section of the signal process is proportional to $1/M_S^{\delta+2}$ [see Eq. (2.10) and (2.11)], so the SB value is proportional to $1/M_S^{\delta+2}$, too. If we suppose that the signature can be detected only when SB $\geq$ 5 in experiment, then we can reach the conclusion that in the case of $\sqrt{s} = 1$ TeV, $\delta = 3$ and unpolarized photon beams, graviton signal can be detected when $M_S \leq$ 2.67 TeV, while in the case of $\sqrt{s} = 500$ GeV, the graviton signal can be detected only when $M_S \leq 1.40$ TeV. These limits are increased to 2.79 TeV (when $\sqrt{s} =$ 1 TeV) and 1.44 TeV (when $\sqrt{s} = 500$ GeV) in $+-$ polarized photon collision mode with $P_\gamma = 0.9$, respectively.

IV. SUMMARY

In this paper we calculate the cross sections for the process $\gamma\gamma \to e^+e^-G_n$ in different polarized photon collision modes, and present some strategies to discriminate the graviton signal from numerous SM backgrounds.

At the stage of ILC with $\sqrt{s} = 1$ TeV, the cross section for the process $\gamma\gamma \to e^+e^-G_n$ can reach several hundred fb. Because the spin of the emitted graviton is 2, the $\gamma\gamma$ collision with $J = 2$ strongly enhances the production rate

TABLE III. Event selection on background and signal ($\delta = 3$), with $+-$ polarized photon beams ($P_\gamma = 0.9$).

	$\sqrt{s} = 500$ GeV				$\sqrt{s} = 1000$ GeV			
	$e^+e^-G_n$	WW	$\tau\tau$	e^+e^-Z	$e^+e^-G_n$	WW	$\tau\tau$	e^+e^-Z
N before cut	5926	96 159	38 271	1340	47 400	99 065	10 299	480
N after $CUT1$	2104	5152	0	59	21 524	631	0	19
N after $CUT2$	1782	3268	0	59	...	...	...	...
Efficiency ϵ	30.1%	3.40%	0%	4.40%	45.4%	0.64%	0%	3.96%
SB		30.89				844.2		

of process $\gamma\gamma \to e^+e^-G_n$, especially when the number of extra dimensions is large. Of course, the cross section increases with the increment of c.m.s. energy $\sqrt{s}$, because more KK states exist which contribute to the cross section. Another effect of the LED shown in this paper is that the cross section decreases when the number of extra dimensions δ goes up.

For the case of $\delta = 3$, we present some strategies to select graviton signals from the numerous SM backgrounds. Because most of the e^+e^- pair of the background processes are back-to-back, taking cut on the open angle between electron and positron can reduce the backgrounds efficiently. With our suggested event selection criteria, we can reach a rather high SB value. We conclude that, by adopting an unpolarized $\gamma\gamma$ collision machine with $\sqrt{s} =$ 1 TeV in the case of $\delta = 3$ and $\mathcal{L} = 100$ fb^{-1}, the graviton signal can be detected when $M_S \leq 2.67$ TeV, while in the case of $\sqrt{s} = 500$ GeV, the graviton signal can be detected only when $M_S \leq 1.40$ TeV. If we adopt a $\gamma\gamma$ collider machine in $+-$ polarized photon collision mode, the detecting upper limits on the fundamental scale can be improved up to 2.79 TeV when $\sqrt{s} = 1$ TeV, and 1.44 TeV when $\sqrt{s} = 0.5$ TeV.

ACKNOWLEDGMENTS

This work was supported in part by the National Natural Science Foundation of China, the Education Ministry of China, and a special fund sponsored by Chinese Academy of Sciences.

[1] N. Arkani-Hamed, S. Dimopoulos, and G. R. Dvali, Phys. Lett. B **429**, 263 (1998); I. Antoniadis, N. Arkani-Hamed, S. Dimopoulos, and G. R. Dvali, Phys. Lett. B **436**, 257 (1998); N. Arkani-Hamed, S. Dimopoulos, and G. R. Dvali, Phys. Rev. D **59**, 086004 (1999).
[2] J. D. Lykken, Phys. Rev. D **54**, R3693 (1996).
[3] E. Witten, Nucl. Phys. **B471**, 135 (1996).
[4] P. Horava and E. Witten, Nucl. Phys. **B460**, 506 (1996); **B475**, 94 (1996).
[5] I. Antoniadis, Phys. Lett. B **246**, 377 (1990).
[6] L. Randall and R. Sundrum, Phys. Rev. Lett. **83**, 3370 (1999); **83**, 4690 (1999).
[7] D. J. Kapner, T. S. Cook, E. G. Adelberger, J. H. Gundlach, B. R. Heckel, C. D. Hoyle, and H. E. Swanson, Phys. Rev. Lett. **98**, 021101 (2007).
[8] G. F. Giudice, R. Rattazzi, and J. D. Wells, Nucl. Phys. **B544**, 3 (1999).
[9] T. Han, J. D. Lykken, and R. J. Zhang, Phys. Rev. D **59**, 105006 (1999).
[10] G. Weiglein *et al.* (LHC/LC Study Group), Phys. Rep. **426**, 47 (2006).
[11] E. A. Mirabelli, M. Perelstein, and M. E. Peskin, Phys. Rev. Lett. **82**, 2236 (1999).
[12] M. Besancon, arXiv:hep-ph/9909364.
[13] S. Dutta, P. Konar, B. Mukhopadhyaya, and S. Raychaudhuri, Phys. Rev. D **68**, 095005 (2003).
[14] D. Atwood, S. Bar-Shalom, and A. Soni, Phys. Rev. D **61**, 116011 (2000).
[15] K. m. Cheung and W. Y. Keung, Phys. Rev. D **60**, 112003 (1999).
[16] V. I. Telnov, arXiv:physics/0512048; Acta Phys. Pol. B **37**, 633 (2006).
[17] A. V. Pak, D. V. Pavluchenko, S. S. Petrosyan, V. G. Serbo, and V. I. Telnov, Nucl. Phys. B, Proc. Suppl. **126**, 379 (2004).
[18] K. Hagiwara *et al.*, Phys. Rev. D **66**, 010001 (2002).
[19] T. Sjostrand *et al.*, Comput. Phys. Commun. **135**, 238 (2001).